Journal of The
Electrochemical Society

Methods for Quantitative Thermal Analysis of Lithium Solid-State and Beyond Battery Safety

To cite this article: Bhuvsmita Bhargava *et al* 2024 *J. Electrochem. Soc.* **171** 110525

Journal of The Electrochemical Society, 2024 **171** 110525

Methods for Quantitative Thermal Analysis of Lithium Solid-State and Beyond Battery Safety

Bhuvsmita Bhargava,[1,=] Nathan Brenner Johnson,[2,=] Alex M. Bates,[2] Loraine Torres-Castro,[2,*] and Paul Albertus[1,*,z]

[1]*Department of Chemical and Biomolecular Engineering, University of Maryland at College Park, Maryland 20740, United States of America*
[2]*Power Sources R&D, Sandia National Laboratories, Albuquerque, New Mexico, United States of America*

The use of differential scanning calorimetry (DSC) to measure the thermal behavior of individual components and electrolyte/electrode combinations is common. However, here we focus on DSC tests on an anode, cathode, and electrolyte (ACE) component combination over a temperature range that includes many of the phase transitions and key reactions (i.e., to 500 °C) that contribute to thermal runaway. This method can help quantify the complex reaction network in a full cell, thereby informing potential safety issues. Here, we used DSC heat flow data from a solid-state $Li_{0.43}CoO_2$+C+PVDF | LLZO | Li metal ACE sample and its components to quantify key factors affecting results. We focused on three areas: (1) ACE sample preparation and assembly in DSC pans, (2) DSC measurement parameters, and (3) heat flow analysis. Key points include the choice of component ratios (e.g., commercially relevant N:P capacity ratio), the importance of conductive carbon and binder, type of pan used, DSC ramp rate, and integration method used when dealing with broad and overlapping exothermic peaks. This work deepens the scientific basis and best practices for obtaining heat flow data from ACE samples for early-stage evaluation of solid-state and beyond battery safety.
 [DOI: 10.1149/1945-7111/ad92e5]

Manuscript submitted August 9, 2024; revised manuscript received November 6, 2024. Published November 28, 2024.

Supplementary material for this article is available online

Lithium Metal Solid State Batteries (Li-SSB) have the potential to increase gravimetric and volumetric energy density vs current NMC811/Graphite Li-ion batteries (LIBs), particularly for applications sensitive to specific energy. They are assumed to be safer than LIBs as they replace flammable liquid electrolytes with non-flammable solid electrolytes. However, recent studies have challenged this assumption.[1–7] In a thermodynamic assessment of Li-ion baseline chemistries vs solid-state batteries, Bates et al. found that under specific situations, such as a short circuit, the total temperature rise in a solid-state battery can be higher than in a LIB.[2] This was also demonstrated by a modeling study by Johnson et al., where a 400 Wh/kg Li_yCoO_2/LLZO/Li solid-state battery reached a temperature of ∼1000 °C.[8] Furthermore, experiments on the stability of solid oxide ceramic electrolytes and sulfide electrolytes with Li-metal have shown high heating rates of 20,000–60,000 °C min^{-1} in some cases.[5,9] While switching to non-flammable solid electrolytes can increase the onset temperatures of thermal-runaway-driving reactions and eliminate combustible liquid electrolyte (thereby preventing the venting of flammable gases that result in fires external to the cell),[10] the increased specific energy, the instability of the lithium metal anode, and the lower specific heat of solid vs liquid electrolytes can still plausibly lead to thermal runaway in Li-SSB. See Table I for the descriptions of abbreviations used in this the article.

Differential scanning calorimetry (DSC) offers a path to study material and component safety at an early stage of cell development, before direct testing on large-format cells can be carried out, and thereby guide R&D towards safer materials and component designs. The information from DSC includes the total heat released, onset temperatures, rates of heat release, and kinetics of reactions between cell materials. In this article we use the term "components" to define battery components like cathode, anode and electrolyte that may be composites of several different "materials." Since DSC samples are typically <0.1 g, this work can be safely carried out at a laboratory scale with low cost. DSC has been extensively used to study the thermal behavior of components, including cathodes and anodes,[11–14] and their interactions with electrolytes.[5,15–17] A detailed description of the working principles of a heat flux DSC can be found in the Appendix. Most studies that use DSC for battery components and materials only study cathode-electrolyte and anode-electrolyte interactions, with a focus on the onset temperature of instabilities, due to reduced complexity of heat flow measurement and analysis, and because the studies are focused on developing a single component (e.g., an electrode or electrolyte material). While these tests are helpful for understanding thermal stability of individual electrodes or electrodes with electrolytes, they do not provide information on heat flow when both the electrodes are present with the electrolyte, and therefore miss the electrode "crosstalk" reactions.[5] DSC tests done on anode (negative electrode), cathode (positive electrode), and electrolyte materials (with or without current collectors) provide important information about the thermochemical pathways and exothermic reactions that result from the interactions of cells. However, measurement and analysis of such tests is difficult because the reactions can result in broad and overlapping heat flows. We refer to the anode, cathode, and electrolyte assembled in appropriate mass ratios in a DSC pan as an ACE sample. ACE-type DSC tests were first (to our knowledge) done by Inoue et al. in 2017[1] and since then only a couple of studies have used this approach to test early-stage safety of LIBs[18] and Li-SSB.[3]

Figure 1 describes the steps to measure DSC heats flow on an ACE sample to obtain information like onset temperatures and total heat release, which can be used to determine the thermochemical reaction pathway for the ACE chemistry.

In this article, we present our experimental and analysis methods to quantify the error and obtain consistent and meaningful results for ACE samples in a DSC. We use the results from our $Li_{0.43}CoO_2$(C+PVDF) | LLZO | Li metal ACE samples in a 1:1 N:P capacity ratio (capacity ratio of the negative to positive electrode)[3] assembled in high-pressure stainless-steel pans as a case study for our methods. While we use this specific chemistry to show how a range of experimental parameters affect the measured heat flow, the methods discussed in this paper also describes the underlying logic and best practices that we have learned while working with other chemistries, such as high-Ni layered metal oxide cathodes, transition

=Equal contribution.
*Electrochemical Society Member.
zE-mail: albertus@umd.edu

Table I. List of abbreviations.

Abbreviation	Description
ACE	Anode-Cathode-Electrolyte (Anode = Negative electrode and Cathode = Positive electrode in this work)
C	Conductive Carbon used as an electrode component
DMC	Dimethyl carbonate
DSC	Differential Scanning Calorimetry
EC	Ethyl carbonate
Li-SSB	Lithium metal Solid-State Battery
LIB	Li-ion Battery
LLZO	$Li_{6.4}La_3Zr_{1.4}Ta_{0.6}O_{12}$ solid electrolyte (LLZO)
N:P Ratio	Negative:Positive electrode capacity ratio (Equivalent to Anode:Cathode capacity ratio)
NMC	$Ni_xMn_yCo_{1-x-y}O_2$
PVDF	Polyvinylidene fluorine
SOC	State of Charge
TGA	Thermogravimetric Analysis

metal fluoride conversion cathodes, and sulfide solid electrolytes. In the broader context of the safety of large format cells, the ACE DSC test methodology presented in this paper can be used to evaluate how changes in electrode composition (e.g., use of pre-lithiation of Si anodes), electrolyte composition (including additives), cell design (e.g., N:P ratio), and other components (e.g., separator, current collectors) can quantitively affect key safety metrics, such as onset temperature and total heat release, without having to make large-format cells for conventional safety testing. The larger context for how our work fits into battery safety evaluation is more fully described in an article by Bates et al.[19]

We follow the sequence of steps shown in Fig. 1 in the following sections. We first report our experimental methods for the $Li_{0.43}CoO_2$(C+PVDF) | LLZO | Li metal ACE samples preparation used in this study, and their heat flow measurements. We discuss the factors to be considered while working with high-pressure closed pans, specifically the impact of reactions involving gas release on pressure inside the pan. Finally, we discuss in detail the implications of the following methods categories:

(i) ACE sample preparation and assembly in pans—This section details the importance of the component mass ratios, handling of cell components (especially Li metal and cathode sheets), and the orientation of components during assembly.
(ii) DSC measurement parameters—This section describes DSC protocols such as heating rate, calibration methods and empty-pan heat flow measurements, which are required for accurate heat flow measurement from ACE samples.
(iii) Heat-flow analysis—In this section we present various baselining methods and analyze their impact on the integration of heat flow to obtain total heat released.

Our Experimental Methods for the $Li_{0.43}CoO_2$ (C+PVDF) | LLZO | Li Metal Chemistry

Sample preparation.—Throughout this paper we use the $Li_{0.43}CoO_2$ (C+PVDF) | LLZO | Li metal chemistry as a case study to demonstrate the effects of sample preparation, DSC measurement procedures, and heat flow analysis on DSC results. We carried out all sample preparation in an Argon-filled MBraun glovebox. For most of our ACE samples, we used $LiCoO_2$ cathode sheets purchased from NEI Corporation that consisted of 90 wt% $LiCoO_2$, 5 wt% Super P conductive carbon, and 5 wt% PVDF binder on a 16 μm aluminum current collector. The cathode sheets were separately charged against a lithium metal anode using 1 M $LiPF_6$ in 1:1 volume ratio of ethylene carbonate (EC)/dimethyl carbonate(DMC), using a polypropylene/polyethylene Celgard trilayer separator. They were delithiated at a rate of C/10 and held at a constant voltage of 4.3 V vs Li until the current dropped below C/100, which corresponded to a lithium content of $Li_{0.43}CoO_2$. The cathode sheets were removed from the split cell after delithiation, drip-washed with diethyl carbonate solvent >10 times

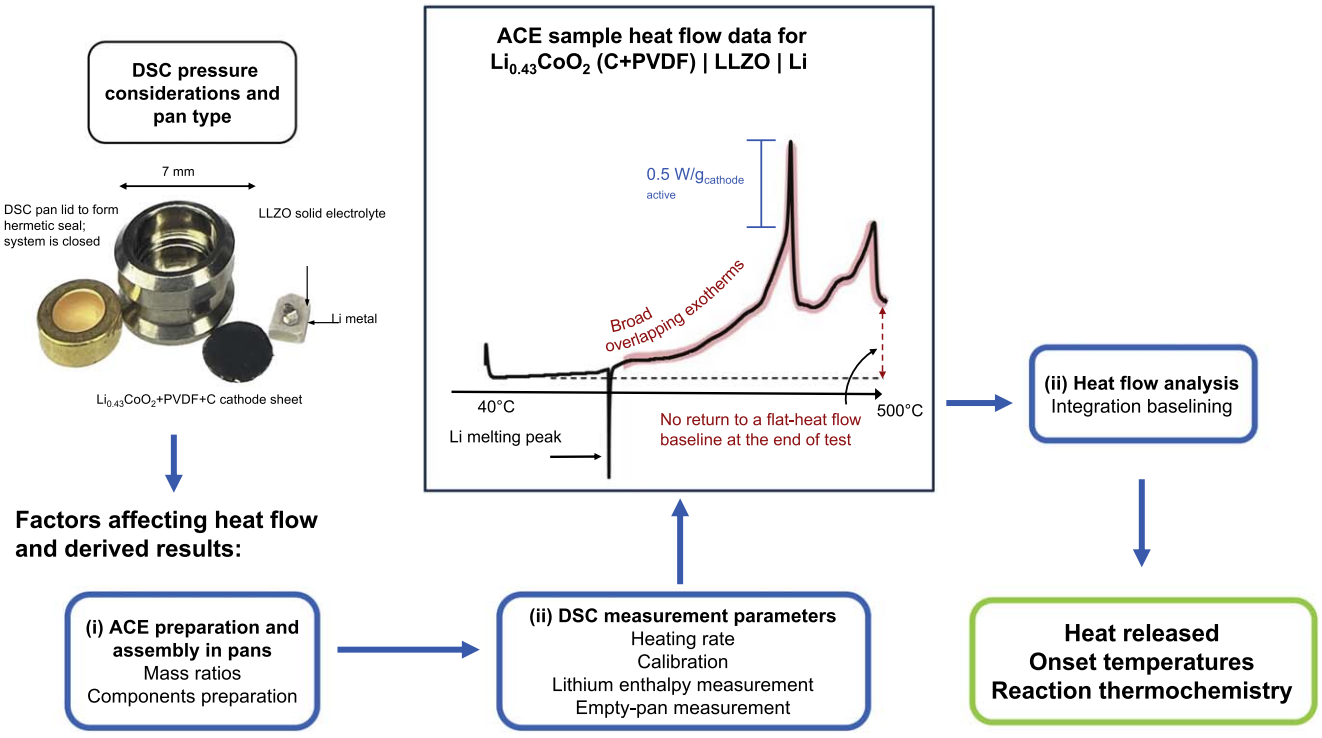

Figure 1. An overview of an ACE sample DSC heat flow measurement. The heat flow curve in the center shows overlapping heat flows and continuous exotherms with no regions without any obvious exotherms at the end of test, which makes analysis challenging. Arrows indicate the order in which each of the steps and events occur.

approximately using 1–5 ml solvent each time, and dried overnight in a vacuum oven at 70 °C.

Component assembly in DSC pans.—Before assembling in the DSC pans, cathode sheets were cut into 4 mm diameter circles (∼0.25 mAh per cutout) with a punch. $LiCoO_2$ cathode sheets with 2 wt% PVDF and 8 wt% C used for specific ACE tests were also purchased from NEI Corp and prepared similarly. 700 μm thick LLZO pellets made by Ampcera and purchased from MSE Supply were fractured into pieces with a weight range of 8–12 mg. Lithium metal with a purity of >99.9% was purchased in the form of Li ingots immersed in light mineral oil was purchased from Sigma-Aldrich. Lithium preparation was done by carefully removing mineral oil smeared edges from a small Li piece that was sliced from the Li ingots, and sharp tweezers were then used to obtain ∼ 150 μg of lithium which was accurately weighed using a micro-balance with a precision of 0.001 mg inside the glovebox. Due to the difficulty in accurately slicing the correct size of Li metal, and variations in the cathode loading, the N:P capacity ratio is generally within +/−10% of 1:1. For the assembly of the ACE samples, the lithium metal piece (∼150 μg) was first placed at the bottom of the DSC pan followed by a piece of LLZO (8–12 mg), and then 2 cutouts of 4 mm diameter cathode sheets (total of 5 mg) charged to $Li_{0.43}CoO_2$ (rinsed and dried) were placed inside the pan. The cathode sheets were placed with the active material side facing the LLZO pieces.

DSC testing procedure.—For all ACE samples, we used SWISSI F20 high-pressure stainless-steel pans with a 20 μl volume purchased from Fauske & Associates. Once the samples were assembled in the pan inside the glovebox, a hand-press with an appropriate die set was used to hermetically seal the F20 pans. Once assembled, the ACE samples were tested in a calibrated Discovery DSC 25 by TA Instruments, at a heating ramp rate of 2 °C min^{-1} from 40 to 500 °C.

DSC Pressure Considerations and Pan Type

It is crucial to consider the pressure-rise from gas generation during testing to avoid pan seal rupture and to ensure that the kinetic conditions for reactions involving gases are relevant. The rate of temperature rise of a battery during internal self-heating and thermal runaway are largely driven by the exothermic reactions occurring among cell components and their materials. In Li-SSB, as the cell heats, phase transitions and/or reaction of cell components can result in gas generation. This gas can then participate in crosstalk reactions with other cell components such as the lithium metal anode. For example, at ∼ 150 °C–200 °C layered metal-oxide cathodes like Li_xCoO_2, and $Li_xNi_yMn_zCo_{1-y-z}O_2$ begin to release oxygen that can react with the lithium metal anode, solid electrolyte and other components present in the cell.[4,9,16,20] Solid/gas reactions have also been reported to occur as the cell self-heats, between oxygen from the cathode and solid electrolytes (especially sulfide electrolytes),[6,21] and these reactions can lead to further gas generation in the DSC pan. For the $Li_{0.43}CoO_2$ cathode with conductive carbon and binder in the ACE sample, two 4 mm diameter cathode sheets were used in the DSC pans. The cathode sheets had a total mass loading of ∼12 mg cm^{-2} and two 4 mm diameter pieces were required to maintain a N:P ratio of 1:1 with the lithium metal anode. Based on this amount, O_2 loss from layered $Li_{0.43}CoO_2$ as it transitions to the rock salt phase results in 0.19 mole O_2 per mole $Li_{0.43}CoO_2$ following the stoichiometry of equation 1 (see Table II). The released O_2 can form CO_2 from a reaction with conductive carbon. Gas-phase HF from PVDF binder breakdown can also contribute to a pressure rise in the DSC pan. While some of these gases may react to form solid-phase species (e.g., $2Li+1/2O_2 \rightarrow Li_2O$), if the O_2/CO_2 and HF remain in the gas phase, ∼40 bar of pressure in the DSC pan at ∼400 °C may be reached for the specific sample masses and pan that we used. Significantly higher pressures can be reached as more sample material is added into the pan. Pressure rise in the pan has a non-linear relation to cathode sample mass due to the increasing gas generation and the larger volume occupied by the sample (i.e. less "empty" volume for the generated gas to occupy). We used sealed stainless-steel pans with a formal rating of ∼200 bar pressures up to 400 °C, with the rated pressure decreasing at the higher temperatures but still above our ∼40 bar estimate based on experimental tests we conducted. Differences in thermal resistance from pan materials and wall thickness are corrected by proper DSC calibration and empty-pan heat flow corrections, as explained in later sections. Hence, when selecting a pan the chemical, thermal, and pressure compatibility with the ACE sample materials should be given primary importance. For the ACE materials in this work, only stainless-steel pans can be used, as shown in the next section and in Fig. 2.

Most DSC tests on battery components and materials use sealed DSC pans for testing but in certain situations like simultaneous DSC +TGA (thermal gravimetric analysis), open pans are used.[21] When open pans are used, the loss of reactive gases would result in lower total heat flow than when closed pans retain reactive gases and the pressure rises following their release. Commercial cylindrical and prismatic lithium-ion cells have a safety-vent valve that opens when the pressure exceeds a threshold; for 18650 Li-ion cells this pressure threshold is typically >∼20 bar.[22] Therefore, using closed pans allows us to explore the scenario with no gas venting, and the reactive gases released from a metal oxide cathode drive exothermic reactions. Controlling the internal pressure to no more than 40 bar also ensures that the reaction kinetics in our DSC pan will resemble that of a cell prior to venting. It is important to note that this pressure is form factor specific. The reaction conditions in a high-pressure pan may reflect that of a cylindrical cell, but it may not resemble that of a pouch cell that vents at a much lower pressure.

Methods Category (i): ACE Preparation and Assembly in Pans

In this section we demonstrate the importance of using appropriate component and materials mass ratios in ACE samples, as well as Li metal and cathode preparation. To quantify the variance from sample preparation and assembly, we constructed five identical ACE samples for the $Li_{0.43}CoO_2$ (with conductive carbon and PVDF) | LLZO | Li metal chemistry with a N:P ratio of 1:1. This result is discussed in the methods category (iii) section on heat flow analysis and integration baselining.

Effect of mass ratios in an ACE sample.—In addition to the "Experimental methods for the baseline chemistry and DSC parameters" discussed above, it is important to select the right mass ratios for the components present in ACE samples. In particular, the ratio of anode to cathode active materials should reflect an expected commercial N:P capacity ratio. For Li metal anodes, a higher N:P capacity ratio will have excess Li metal in the system that could lead to higher total heat generation. For instance, for $Li_{0.43}CoO_2$ (with conductive carbon and PVDF) | LLZO | Li metal system, where the cathode is charged to 4.3 V vs Li, the simplified cathode thermal decomposition reaction is given by equation 1 in Table II.

The O_2 from this decomposition can react with Li as given by equation 2 in Table II.

Therefore, for one mole of Co, 0.19 moles of oxygen will be released over a broad temperature range (from ∼170 °C to ∼400 °C) and for an N:P capacity ratio of 1:1, only 0.57 moles of lithium are available, so the O_2 is in excess. The heat released from this reaction could be >25% higher if enough lithium was present to fully react with the O_2 (N:P > 1.33) to form Li_2O. If O_2 is in excess as for the 1:1 N:P ratio, it may react with other components of the cell such as conductive additive and/or binder.

Figure 2a shows the difference in heat flow measurement on the same materials set, Li_xCoO_2 (conductive carbon and PVDF) | LLZO |Li metal but with different N:P ratios. The blue curve shows heat flow measured on an ACE sample with 8.5:1 N:P ratio; the maximum heat flow measured in this case was 4.1 $W/g_{Li0.43CoO2}$ compared to 1.2 $W/g_{Li0.43CoO2}$ for the red curve with an N:P ratio of

Table II. Proposed major reactions occurring in our ACE samples.[3] Negative enthalpy indicates an exothermic reaction.

Equation #	Reaction equation	Theoretical enthalpy adjusted to 400 °C	
1	$Li_{0.43}CoO_2 \rightarrow 0.43LiCoO_2 + 0.19Co_3O_4 + 0.19O_2$	$-150.4\frac{kJ}{mol\ Li0.43CoO2}$	12, 24
2	$4Li + O_2 \rightarrow 2Li_2O$	$-1213\frac{kJ}{mol\ O2}$	
3	$4C + O_2 \rightarrow CO_2$	$-393.5\frac{kJ}{mol\ O2}$	
4	$2Li + HF \rightarrow LiF + LiH$	$-440.3\frac{kJ}{mol\ HF}$	

1:1. The total heat released in the case with 8.5:1 N:P ratio was ~3000 W/$g_{Li0.43CoO2}$ which was ~15% higher than for the 1:1 N:P case. With an N:P ratio of 8.5:1 there is sufficient lithium for complete reaction with both oxygen released from $Li_{0.43}CoO_2$ and with HF released from the PVDF binder (equation 4), while for the 1:1 N:P ratio case the system has excess oxidant (oxygen, HF) vs lithium.

Other important factors that can impact oxygen evolution and heat flow in case of commercial layered metal cathodes are the Li content of the electrode (i.e., SOC), cathode particle morphology and ratio among Ni-Mn-Co and other metals.[12,23] The cathode sheet should also contain commercially relevant mass ratios of conductive carbon and binder additives. Figure 2b compares an ACE sample, $Li_{0.43}CoO_2$(PVDF+C) | LLZO |Li with different amounts of PVDF and C in the cathode; 2% PVDF and 8% C of the total cathode mass (blue) and 5% PVDF and 5% C in cathode (red). The onset temperatures and peak locations remain similar in both cases, but the heats released are significantly different. With 2 wt% PVDF and 8 wt% C the total heat released is ~3240 W/$g_{Li0.43CoO2}$, while for 5% PVDF and 5 wt% C the total heat released value is lower at ~2500 W/$g_{Li0.43CoO2}$. With more carbon in the 8 wt% C case, more of the released O_2 could react with C than Li as given by equation 3 in Table II, and per mole of O_2 the heat release for CO_2 formation is ~3x lower than for Li_2O formation (equation 2). With less Li reacting with the O_2 below 400 °C, this could also explain the larger exotherm at >400 °C as the Li reacts with HF released from binder breakdown given by equation 4 in Table II. For this material set, the mass ratio of LLZO to anode and cathode is not important because LLZO does not participate in any significant exothermic reactions up to 500 °C. However, in cases where reactive solid electrolytes are used, the heat flow could depend on the electrolyte:cathode and electrolyte:anode ratios. In the cases where a reactive electrolyte is used, the surface area to volume ratio of the electrolyte may also affect the heat flow. The amount of electrolyte and the electrode: electrolyte ratio is also important when liquid electrolytes are studied.

Li metal anode handling and preparation.—In addition to the mass ratios, careful material handling and preparation of the cell layers inside a glovebox should be done to avoid composition changes. For the $Li_{0.43}CoO_2$ (with conductive carbon and PVDF) | LLZO | Li metal system, we calculate the amount of lithium removed (in mAh) when the cathode sheets are charged to $Li_{0.43}CoO_2$ or 4.3 V vs Li/Li^+. We use a capacity of 3860 mAh/g_{Li} to obtain the mass of lithium, which we then add (to within ± 10% of the mass needed for a 1:1 N:P ratio) to our ACE samples. The amount of lithium used is ~0.1–1 mg, depending on the N:P ratio and amount of cathode active material. Increasing the amount of lithium while keeping a constant N:P ratio of ~1:1 requires increasing the cathode mass, which is limited by the pressure generated per mole of the cathode and the DSC pan's pressure rating at the temperatures of interest. The small amount of lithium makes it more susceptible to contamination. Even when stored inside a glovebox, lithium metal reacts with the small amounts (0.1–5 ppm) of O_2, CO_2, H_2O and N_2 and forms a surface layer. If a lithium foil is used as the source of the lithium piece, the surface layer must, at the least, be carefully scraped off with a clean blade/brush. However, this carbonate/oxide layer often cannot be completely removed by scraping it off with a stainless-steel brush. As such, more rigorous methods of ensuring lithium purity are required, to obtain as pure of a lithium sample as possible. Changing the form factor of the bulk lithium source to reduce the surface area to volume ratio can help reduce surface contamination. We found that lithium ingots stored in light mineral oil inside the glovebox showed higher purity compared to a thin foil since a clean razor blade could be used to slice off the mineral oil contaminated edges revealing a large amount of pure (99.9%) lithium. The purity of the lithium sample after preparation can be directly measured by comparing the integrated heat flow from lithium melting with the known enthalpy of melting of pure lithium (~435 J/g_{Li}). The lithium used in the ACE sample examples used in this study were prepared using this ingot method and gave a melting enthalpy within ± 3% of the reference value. This method of measuring Li melting enthalpy to check for purity only works if Li does not react with the pan or other materials present below its melting point (180.5 °C).

It is also important to choose a pan that is compatible with the sample material and does not react during testing. Standard aluminum DSC pans alloy with lithium metal and cannot be used (Fig. 2d). Copper foil can be used to separate lithium from the aluminum pan, but lithium also alloys with the copper foil (Fig. 2d) between 300 °C–350 °C. If copper is used in ACE samples as a current collector with a Li metal anode, lithium-copper alloying should be considered in the reaction pathway analysis.

Cathode preparation.—For the purpose of DSC tests, cathode sheets can be reliably charged to the desired Li composition (i.e., SOC) in a coin cell or split cell using standard liquid electrolytes and Li metal as the anode. After charging the cathode sheet, the electrolyte needs to be removed, then washed with an appropriate solvent based on the type of electrolyte used for charging the cathode sheet, and finally dried under vacuum. Some commonly used solvents for removing $LiPF_6$ salt from cathodes are Diethylene Carbonate (DEC), and Dimethyl carbonate (DMC) given their ability to dissolve $LiPF_6$ and their low boiling point of 90 to 100 °C. DSC and Thermogravimetric Analysis (TGA) on cathode sheets prepared with varying washing and drying procedures can be helpful to verify the efficacy of electrolyte removal. Liquid electrolytes that remain in the cathode sheet in a DSC sample would react with oxygen and result in heat flow. Liquid electrolytes have a low boiling point (usually <200 °C), hence, mass loss can be seen in TGA from solvent vaporization. Additionally, liquid electrolytes can drive high-Co and high-Mn cathode decomposition further to rock salt phase species releasing more oxygen whereas many dry cathodes will stop at the spinel phase.[12,25] The two curves in Fig. 2c show results with and without liquid electrolyte present; the maximum heat flow is 0.6 W/$g_{Li0.43CiO2}$ without electrolyte (rinsed and dried) vs 1.6 W/ $g_{Li0.43CiO2}$ with liquid electrolyte present. The onset temperatures of exothermic reactions in each of these cases are also different with earlier onset of the first exothermic peak in the case of cathode with electrolyte. Therefore, any remnant liquid electrolyte can alter the DSC heat flow data and must be carefully controlled, especially for ACE samples with overlapping heat flow peaks. In addition to detecting mass loss from solvent evaporation in cathode sheets, TGA can also be used to

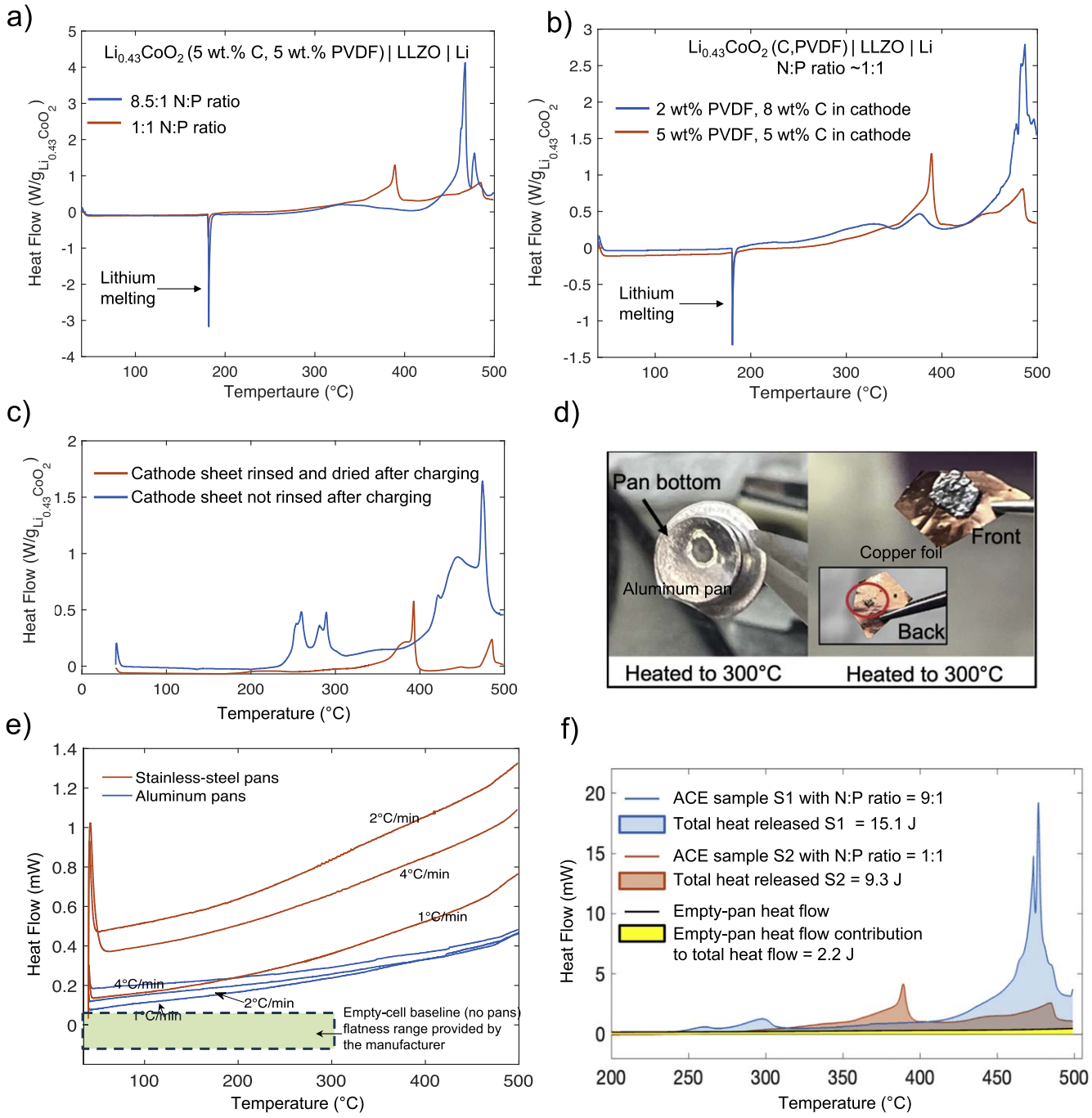

Figure 2. The importance of mass ratios, material handling, and sample preparation for DSC heat flow results, (a) heat flow data for $Li_{0.43}CoO_2$ | LLZO | Li in a 1:1 N:P ratio (red) compared to an 8.5:1 N:P ratio (blue) ACE sample where the total heat flow is higher from increased reaction with the Li metal. (b) heat flow for $Li_{0.43}CoO_2$ + C + PVDF | LLZO | Li in a 1:1 N:P ratio with varying weight% of PVDF binder and conductive carbon in the cathode showing different heat flow behaviors depending on the limiting reactants and the extent of reactions. (c) Un-rinsed and un-dried $Li_{0.43}CoO_2$ cathode sheets show larger exothermic heat flow with an earlier onset temperature due to the presence of residual organic solvents compared to smaller heat release in the case of rinsed and dried cathode. (d) Lithium reaction with aluminum DSC pan (left) and copper foil (right) heated up to 300 °C, demonstrating the need to use a stainless steel pan when using Li metal (e) empty pan heat flow measured with stainless steel and aluminum pans, (f) heat integrated (shaded region) for model $Li_{0.43}CoO_2$ (C+PVDF) | LLZO | Li ACE samples with N:P ratio 1:1 (red) and N:P ratio 9:1 (blue) compared to the apparent heat released in an empty pan test (shaded yellow).

detect mass loss from layered metal oxide cathode decomposition and O_2 release from electrolyte-free cathode sheets.

Methods Category (ii): DSC Measurement Parameters

Once a sample preparation method and pan type have been established based on the ACE sample composition, a DSC testing protocol needs to be developed. In this section, we explain the importance of DSC heating rates, calibration methods, lithium melting enthalpy measurements, and empty-pan heat flow measurements.

DSC heating rate.—\An important parameter to set is the DSC heating rate, in °C/min. A higher heating rate results in higher heat flow, but also lower peak resolution and a greater shift in the peak location. In

addition, the heating ramp rate should consider the sample-to-pan mass ratio and sensitivity of the DSC instrument. For the case of high-pressure stainless steel DSC pans, the sample mass is 2%–3% of the pan mass and thermal lag effects from heat transfer within and through the pan could have a large impact on the measured heat, especially at high ramp rates. The International Confederation of Thermal Analysis and Calorimetry (ICTAC) recommends that the product of the sample mass and the heating rate should be $\leqslant 100$ mg °C min^{-1} and that the sample mass times the heating rate should be kept as constant as possible for kinetic studies.[26] For larger pans, it is better to keep the product of the sample mass and heating rate lower to prevent thermal gradients from developing in the pan and the sample. In such situations, we recommend using heating ramp rates of < 5 °C min^{-1}. For lighter pans, such as standard aluminum pans, the ramp rates may be higher. Generally, having an estimate of the sample-to-pan mass ratio and having an estimate of the rate of heat release of the sample will help in estimating an appropriate scan rate for the tests. The importance of an appropriate ramp rate is further discussed in the heat flow analysis section.

Calibration methods.—Before running the tests in DSC, the instrument must be calibrated using the same type of pans, the same gas purge flow rate, and the same temperature range as used in the actual test. Calibrating a DSC accounts for the thermal resistances of the calorimeter and calorimeter + pan system on both the reference and sample sides. The pan + calorimeter system was modeled in detail by Danley as a set of capacitive (energy storing/heat capacity) and resistive (conductive/convective resistance to thermal transport) components.[27] Appendix discusses this model in detail, which is helpful in understanding uncertainties in heat flows arising from internal resistances and role of calibration steps.

Current state-of-the-art DSCs guarantee a "baseline" flatness in the 20–100 μW range over a stated temperature range (e.g., −50 °C to +300 °C), but it is important to note that this range only accounts for the calorimeter's resistances, i.e. without any pans present. An upper temperature for baseline flatness of 300 °C does not cover the range of interest for battery thermal runaway studies, which for our case is to 500 °C due to the PVDF breakdown temperature. In addition to the empty cell calibration, temperature and cell constant calibrations are required to align, respectively, the onset temperature of a thermal event and the total heat release. While these are two distinct and separate calibrations, they can often be both accomplished with a single run with a standard sample material. However, it is possible to separate these calibrations and perform them on two different standards if needed. The typical calibration material is Indium metal, which has a melting temperature of 156.6 °C and a melting enthalpy of 28.6 J g^{-1}. Calibration involves the specification of parameters to give these values. For the temperature calibration, this adjustment manifests as a shift in temperature, and for the cell constant it is typically a multiplication factor on the measured heat flow values. The cell constant and temperature calibrations must be done at the ramp rate and with the exact pans that will be used to perform testing. Additionally, these calibrations are performed in a small temperature window where the indium phase change occurs (typically ∼10 °C temperature range). The further a sample measurement is done from the indium phase change temperature, the less accurate it may be. Some authors also recommend using multiple calibration standards and performing a multi-point calibration to cover a greater temperature range.[28,29] However, this is not always possible for the entire testing temperature range as very few standard calibration materials are inert at high temperatures and give reliable and repeatable cell constant calibrations. To achieve higher temperatures, ceramic pans (e.g., Al_2O_3) are required but they cannot be hermetically sealed and will also eventually react with lithium metal at temperatures higher than ∼400 °C, making stainless-steel pans the best available option.

Lithium melting enthalpy measurement.—In addition to measuring lithium melting enthalpy to check for lithium metal purity, as mentioned in the lithium anode preparation section above, the hermetically sealed stainless-steel pans offer another advantage; after the DSC ramp test up to 500 °C on ACE samples, a second ramp test (from ∼170 °C–190 °C) can be run on the same ACE sample pan to measure the melting enthalpy of any unreacted lithium from the previous ramp test. We call this a Li remelt test. For all the ACE samples shown in this paper we do not observe a lithium melting endothermic peak on the remelt run. This implies that all the lithium was consumed in reactions that occurred in the first ramp test from 40 °C to 500 °C.

Empty-pan measurements to assess the heat flow baseline.—The resistance to heat transfer arising from pan material and pan-to-sensor contact can be accounted for in an additional test where empty sample and reference pans are used to obtain a "zero heat flow" line or empty-pan heat flow. Ideally, if the resistances and capacitances on both sides are equal, the empty pan heat flow should be zero, therefore a non-zero empty-pan heat flow is obtained when the resistances are not equal. Additionally, while all DSCs account for the empty cell baseline through routine calibrations, most do not account for an empty pan baseline. This adjustment typically will need to be done by the user during post-test data processing. As discussed in detail in the next section, the empty-pan heat flow can be subtracted from the measured sample DSC heat flow as part of this analysis.

In our empty-pan tests we typically observe positively sloped heat flow i.e. increasing heat flow with increasing temperature. This is attributed to a temperature dependent change in the thermal resistance between the reference/sample sensor and the reference/sample pan not accounted for in calibration. As can be seen in Fig. 2e, the slope of the empty-pan heat flow was larger for the high-pressure stainless-steel pans (which weigh ∼900 mg) used in this study vs standard aluminum pans (which weigh ∼50 mg). The thermal conductivity of stainless-steel is five times lower than aluminum. The stainless-steel pans are also much thicker than the standard aluminum pans, which can affect the heat transfer between the sample and sensor. A non-zero empty-pan heat flow poses a challenge to identify and quantify the true sample heat flow. The empty reference pan was the same throughout all our tests and we assume that its thermal properties do not change, however the contact resistance between the pan and pedestal could be slightly different for each run. The extent of this variation is dependent on the efficacy of the calibration and instrument design. For instance, a difference in the baseline heat flow in heat flows was observed in ACE samples and cathode-only samples when run on a TA Discovery DSC 250 vs the Discovery DSC 25. The 250 DSC uses a more robust model with fewer assumptions (referred to as the T_{zero} heat flow model) to estimate the internal resistances and capacitances (shown in Fig. A.2) of the calorimeter. This could be one explanation of the lower apparent baseline heat flow in this system. Fig. S3 (supplementary information) compares the apparent baseline heat flow in ACE and cathode only samples on the TA Discovery DSC 25 and TA Discovery DSC 250.

To separate the sample and empty-pan baseline heat flows, it is helpful to increase the magnitude of the sample heat flow. This can be done by increasing the mass of active components (such that the pressure is less than the pan's rating) in the cell and/or by increasing the heating ramp rate. To demonstrate this point, an ACE sample with an N:P capacity ratio of 9:1 was constructed by increasing the amount of lithium in the pan. Figure 2f shows heat flow differences between the ACE sample with 9:1 N:P ratio (sample S1) and an ACE sample with 1:1 N:P ratio (sample S2). Increasing the amount of lithium metal resulted in higher heat flow with a maximum of 18 mW in S1 vs a maximum heat flow of ∼4 mW in S2. The shaded region in yellow is the apparent heat released from an empty-pan heat flow test. The total heat in S1 was 15.1 J which is much higher than for S2 (9.3 J). The heat contribution from the empty-pan baseline contribution to the total heat was 2.2 J, which was ∼14% of the total heat from S1 compared to ∼23% of total heat released in

S2. Accounting for the contribution of the empty-pan heat flow during data analysis is discussed in detail in the next section.

Methods Category (iii): Heat Flow Analysis

In the present section we discuss the analysis of heat flow data, and in particular the integration of heat flow data. Figure 3 shows the heat flow from an ACE sample composed of $Li_{0.43}CoO_2$ (C+PVDF) | LLZO | Li metal from 40 °C to 500 °C, several approaches for integration, and the results of integrations including accounting for the impact of empty-pan heat flow. Relevant data is also provided in Table III. The heat flow in Fig. 3a is the result of the endothermic lithium melting at ∼180 °C and several exothermic kinetic events (e.g., cathode decomposition, reaction of O_2 with conductive C and lithium metal, reactions involving HF from binder). The composition and heat capacity of such a system evolves as gases are released and new solid products form. The chemical reactions happen over a broad temperature range (i.e., 10 s to 100 s of °C) and are dependent on the kinetic conditions and the mass and energy transport within the sample. For example, in Fig. 3a, only two sharp exothermic peaks are observed at ∼380 °C and ∼470 °C, but a broader exothermic region extends from ∼170 to 500 °C, likely resulting from reactions due to continued oxygen release from $Li_{0.43}CoO_2$ up to 400 °C.[30] To quantitatively analyze the heat flow derived from such a system becomes challenging, as there is no return to a "transition-free heat-flow" region at the end of the test that would indicate reaction completion. We define a "transition-free heat flow" region as a temperature range in which exothermic or endothermic peaks from kinetic transitions or phase transitions are absent, resulting in a constant slope for heat flow vs temperature. For example, in the specific ACE case shown in Fig. 4, the transition-free heat flow region is between 50 °C to ∼165 °C (before lithium melting endotherm appears). It should be noted that transition-free heat flow does not necessarily imply zero heat flow. Without a transition-free heat flow region at the end of the test, integration to obtain total heat released depends on how the baseline for integration line is defined. Several authors recommend having a 10 °C–20 °C trail-off zone where no reactions occur to establish a clear baseline for heat flow integration.[25,31] However, this is not always possible depending on the maximum temperature rating of the pan and the DSC itself.

In the absence of a clear transition-free heat flow region at the end of test, it is generally recommended that prior to running the sample, an

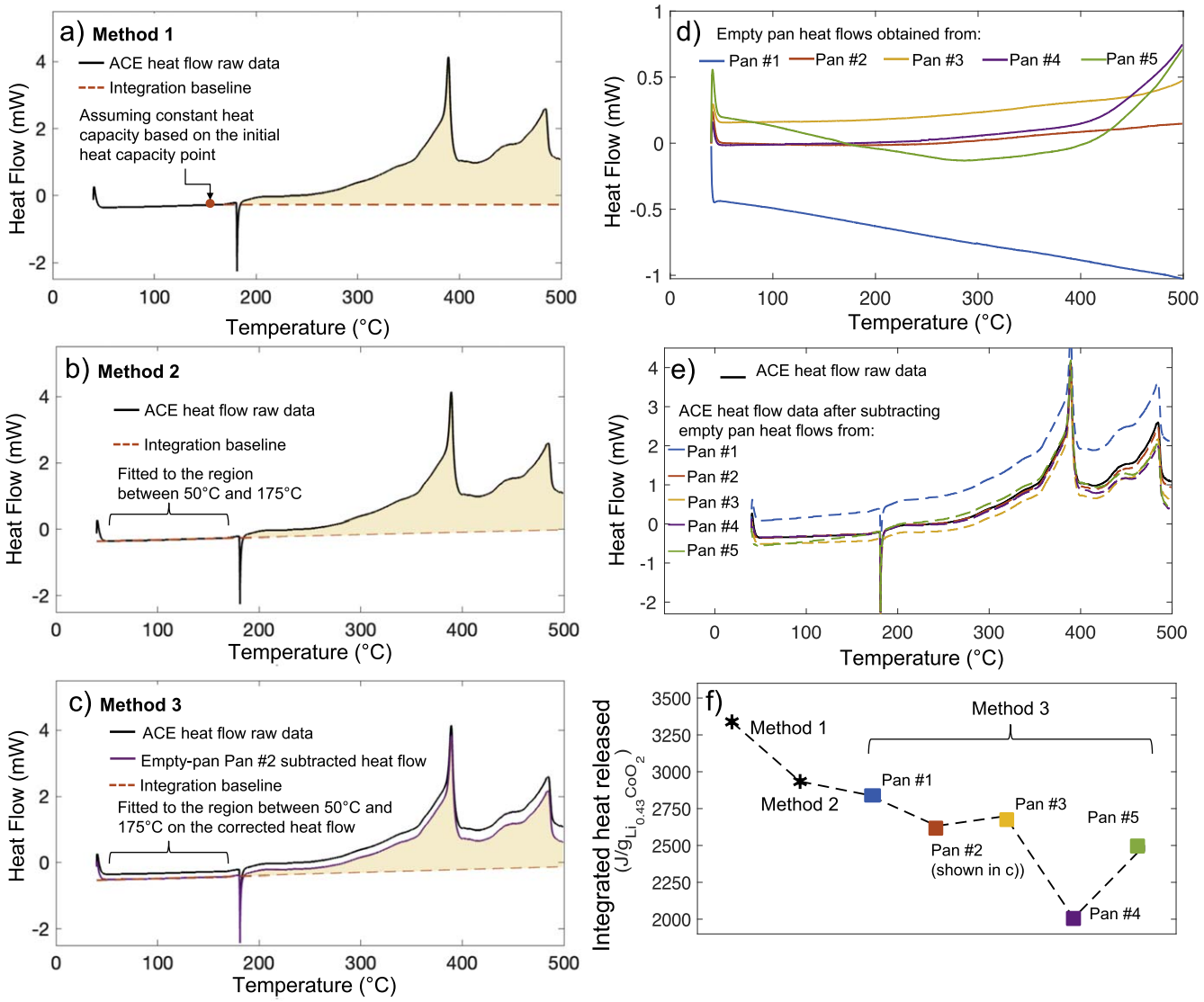

Figure 3. ACE sample (1:1 N:P ratio and $Li_{0.43}CoO_2$ cathode with 5 wt% conductive carbon and 5 wt% PVDF binder) heat flow analysis to obtain total heat released using (a) Method 1—single point (local minima) in the initial transition-free heat flow temperature range between ∼50 to 170 °C and a horizontal integration baseline, (b) Method 2—integration baseline polynomial fitted to the flow region from ∼50 to 170 °C. (c) Method 3 - empty-pan heat flow subtraction followed by integration baseline fitted to the transition-free heat flow region from ∼50 to 170 °C, (d) empty pan-heat flows for five different pans against the same reference pan, (e) corrected ACE sample heat flows after subtracting the empty-pan heat flows, (f) final integrated areas obtained using the three methods.

Table III. Total calculated heat released (in J/g $Li_{0.43}CoO_2$) for five sequentially built $Li_{0.43}CoO_2$|LLZO|Li ACE samples using Method 1, Method 2 and Method 3 for integration baselining. Average values and maximum variation are also provided.

Integration methods	ACE sample #					Average heat released for 5 ACE samples	Maximum variation among 5 ACE samples
	1	2	3	4	5		
Method 1	3340	3018	2663	2881	2995	2979	**25.4%**
Method 2	2934	2747	2492	2655	2685	2703	17.7%
Method 3 Pan #1	2743	2479	2842	2622	2659	2669	14.6%
Method 3 Pan #2	2513	2349	2633	2377	2436	2462	**12%**
Method 3 Pan #3	2502	2334	2699	2380	2551	2493	15.6%
Method 3 Pan #4	1881	1625	2008	1796	1842	1830	23.5%
Method 3 Pan #5	2237	2134	2481	2202	2255	2262	12.6%

empty-pan run should be measured using the same pans intended to be used for the sample test to account for the thermal resistances arising from the pan+DSC system.[31–34] However, this is not always possible, especially for high-pressure pans that cannot be re-opened after sealing. We consider three different integration baselining methods for this case. A schematic description of each of the three integration baselining methods can be found in the supplementary information (Fig. S2).

Method 1 assumes that the sample's heat capacity is constant throughout the test and is most suitable when a clear initial transition-free heat flow region does not exist, and empty pan data cannot be obtained. The integration baseline is obtained by using a single point to define the sample's heat capacity (typically selected before the start of clear exothermic peaks if possible or a local minimum between exotherms). This is demonstrated in Fig. 3a, where the red dot represents the selected point in the transition-free heat flow region, and a straight and horizontal line is used from this point to the end of test as the integration baseline (red dashed curve in Fig. 3a).

Method 2 uses multiple points in regions without any obvious exothermic peaks (referred to as transition-free heat flow regions) to fit a polynomial of the lowest possible order (such that fitted curve

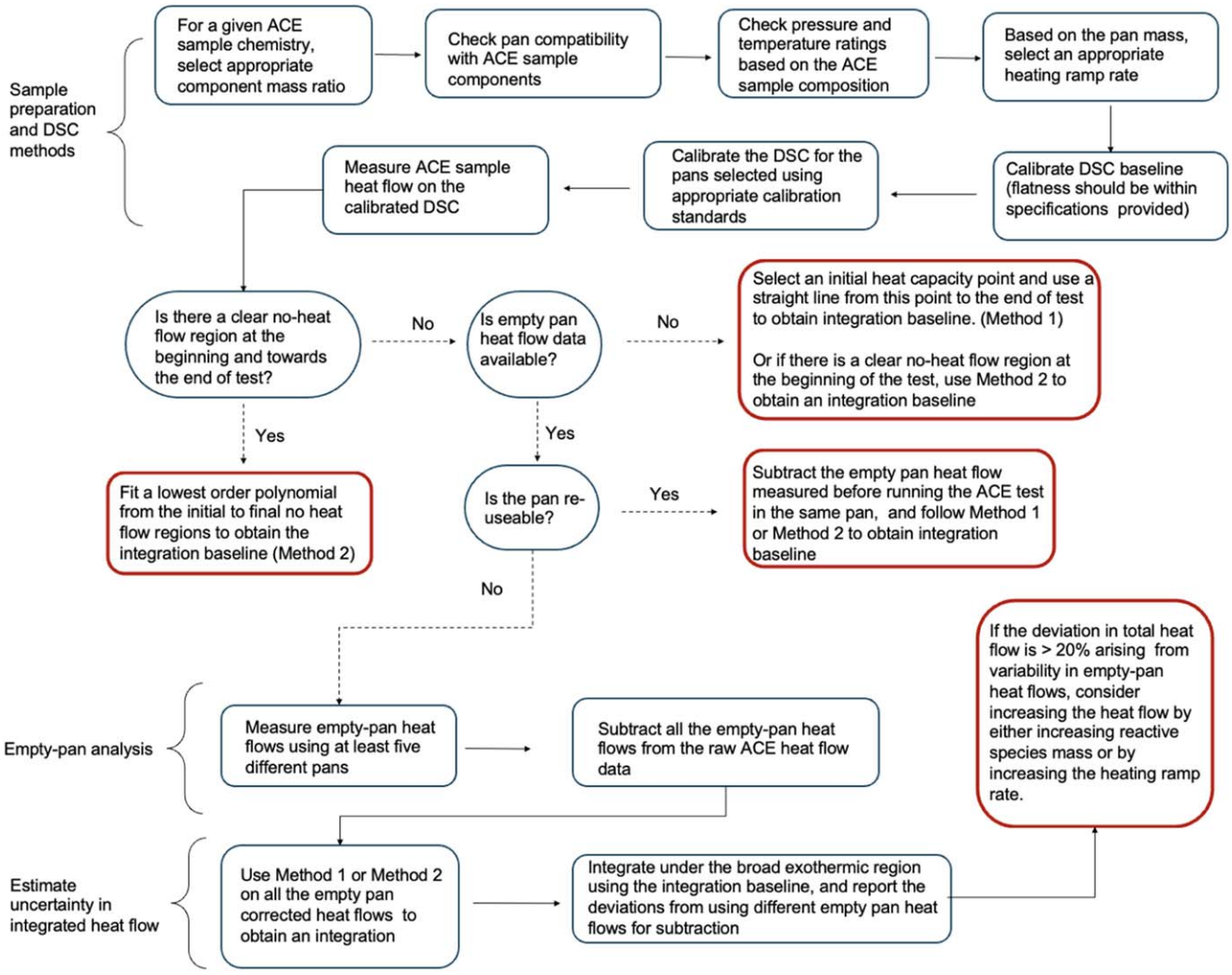

Figure 4. Summary of recommended steps and practices involved in methods including ACE sample preparation, DSC measurement parameters, and heat flow analysis.

does not pass through any of the exothermic peaks) to serve as the integration baseline. This method considers two cases; Case 1 is a when transition-free heat flow region is present at the start of the test, as seen in Fig. 3b between 50 to 170 °C. In this case, points in the transition-free heat flow region should be selected to fit a polynomial baseline. Case 2 is when clear transition-free heat flow regions are present both at the start and towards the end of test. In this case, points on both of the transition-free heat flow regions should be selected to fit a polynomial baseline. See Fig. S3.b for a schematic representation of case 1 and Fig. S3.c for Case 2.

Method 3 considers a case where empty-pan heat flow data can be measured and subtracted from the heat flow curve. Once the empty pan data is subtracted, Method 2 is used on the ACE heat flow data corrected for the empty pan, to obtain an integration baseline as shown in Fig. 3c. Method 3 is especially useful when empty-pan data can be measured prior to running the intended DSC test with a sample in it. However, for pans that can't be reopened, the empty-pan baseline must be determined with pans different than those used for the samples. Therefore, to account for the variabilities in empty-pan heat-flows of the high-pressure stainless-steel pans used in our tests, heat flow from five different empty sample pans (without changing the reference pan) were measured as shown in Fig. 3d. The heat flows and total heat released values after subtracting these five different empty-pan heat flows from an ACE sample heat flow data are shown in Figs. 3e, 3f and Table III. The variation in the measured empty-pan heat flows could be a result of a combination of changing thermal resistances from slight variation in the overlapping area of the pan and the sample thermocouple, internal resistances of the calorimeter thermocouples, slight variations in pan masses (0.5%–1.5%), and contamination at the pan/sensor interface. It should be noted that no direct correlation was observed between empty pan heat flow and pan mass in this range of mass variability between the pans.

To quantify variance arising from ACE sample preparation and assembly, we used the three baselining methods listed above for five sequentially built ACE samples. These samples have the same components ($Li_{0.43}CoO_2$ (C+PVDF) |LLZO|Li), the same cathode sheet composition, the same N:P capacity ratios, and the same mass ratios (to the practical limit of weighing). Further, all these samples were all built in the same glovebox conditions. The variability in the total exothermic heat release for the five individually assembled ACE samples for the three integrations Methods are reported in Table III. In addition, the results in Table III for Methods 1 to 3 for ACE sample #1 are shown in Fig. 3f.

Table III provides quantitative information on both variance in total heat release among sequentially prepared samples, and variance in the average total heat release among Methods 1 to 3 for the set of sequentially prepared samples. First, we see that the variance in total heat release among sequentially prepared samples ranges from about 12% to 25% depending on the heat flow analysis method. This appears to be the approximate floor of the expected variance among a set of sequentially prepared samples using the full set of our methods, from sample preparation to DSC measurement parameters to heat flow analysis methods. While Method 3 has lower variance among samples than Methods 1 or 2 (for 4 of the 5 empty pans), we do not believe that this lower variance is alone enough to justify a recommendation for the use of Method 3. Second, Table III shows that Method 1 produces the largest average heat release (2979 $J/g_{Li0.43CoO2}$), while Method 3 with empty pan heat flow from Pan #4 (Method 3-Pan #4) results in the lowest value (1830 $J/g_{Li0.43CoO2}$). This is a substantial difference of >60%. However, comparing the average heat release from Method 1 (2979 $J/g_{Li0.43CoO2}$) with the average heat release from Method 3 (averaging over the 5 empty pan baselines and giving 2343 $J/g_{Li0.43CoO2}$) gives a difference of about 27%. This directly shows the importance of using multiple empty pans when applying Method 3. Summing up the results in Table III, we find the variation among 5 sequentially prepared pans for a single integration method can reach about 25%, and the variation among the average values for the three methods can reach about 27%. An earlier section of this paper describes the variance in component masses during sample preparation, which generally result in about +/−10% variation from 1:1 for N:P capacity ratio. However, our analysis shows the variation in N:P ratios among the five ACE samples does not explain the variation in their total heat release. We believe that the remaining variances in total heat released are inherent to the ACE system and are a result of the stochastic nature of gas-solid reactions that are sensitive to the surface solid properties and partial pressures of the reacting gases.

Figure 4 shows key considerations and our recommended best practices in ACE sample preparation, assembly, DSC testing and finally heat flow analysis. The flowchart considers several conditional statements related to the presence of heat-flow regions (temperature ranges >10 °C–20 °C) with no exothermic peaks, the availability of empty-pan heat flow data, pan re-usability, and others. Final recommendations are included in termination step for each of the test cases discussed.

Conclusions

While DSC analysis is extensively used in the battery field to assemble material thermal stability and compatibility with other materials, there is a critical gap in methods for the use of this analysis technique for samples that include at least an anode, cathode, and electrolyte. This gap in methods adds difficulty in measuring accurate DSC heat flows and analysis to obtain meaningful parameters, for example the onset temperatures of key reactions and the total heat released. In this study we present an analysis and best practices for this approach, using a case-study of a specific solid-state lithium metal with metal oxide cathode ($Li_{0.43}CoO_2$ (C+PVDF)/LLZO/Li metal) material set, and sharing our measurements on how variations in the methods impact the resulting heat flows. We include measurements on and a discussion of uncertainties with respect to both sample-to-sample variations and the choice of integration baseline. We observed that sample to sample variation in total heat released among identically built ACE samples is up to ∼25% for a given integration method, while the variation of the average total heat released among the three integration methods is up to about 27%. In this paper we have summarized ways of minimizing some of these factors contributing to the variations, giving particular attention to ACE sample preparation and assembly (e.g., pan choice, ratio among components), DSC measurement parameters (e.g., heating rate, calibration), and heat flow analysis (e.g., how to define an integration baseline when there are broad and overlapping exotherms and no return to a transition-free heat flow condition at the end of the test). The methods presented here can be used to carry out ACE tests on Li-ion-based chemistries with liquid electrolytes, or on solid-state cells with reactive sulfide solid-electrolytes, as discussed in a recent article published in ECS Interfaces on ACE DSC tests.[19] We believe that this paper will serve as an important guide for future DSC experiments conducted on ACE battery samples and help advance the practice of predicting the safety of next-generation battery chemistries at the materials and component stage of research and development.

Acknowledgments

B.B., N.J., and P.A. completed the significant majority of the experimental, analysis, and writing work for this paper with the support of the DEVCOM Army Research Laboratory (ARL) under Cooperative Agreement Numbers W911NF-20–2–0284 and W911NF-22–2–0021. A.B., L.T.C., and N.J. provided feedback on the work and editing of the writing based upon work supported by the U.S. Department of Energy, Office of Electricity (OE), Energy Storage Division. The views and conclusions contained in this document are those of the authors and should not be interpreted as representing the official policies, either expressed or implied, of the Army Research Office or the U.S. Government. Sandia National

Laboratories is a multi-mission laboratory managed and operated by National Technology and Engineering Solutions of Sandia, LLC., a wholly owned subsidiary of Honeywell International, Inc., for the U. S. Department of Energy's National Nuclear Security Administration under contract DE-NA-0003525. This paper describes objective technical results and analysis. Any subjective views or opinions that might be expressed in the paper do not necessarily represent the views of the U.S. Department of Energy or the United States Government. The U.S. Government is authorized to reproduce and distribute reprints for Government purposes notwithstanding any copyright notation herein.B.B. was additionally supported by the Harry K. Wells Graduate Fellowship in Energy from the University of Maryland's A. James Clark College of Engineering.

Appendix. Description of the Working Principle of a Heat-Flux DSC Cell

In the present work, we use a heat-flux DSC, the TA Discovery 25. In a heat-flux DSC,[27] the temperatures of a pan with the sample and an empty reference are measured by areal thermocouples, and sample pan heat-flow is calculated from the temperature difference. Both the sample and reference pans are placed inside a temperature regulated furnace referred to as the DSC cell (this is the reference and sample pan compartment shown in Fig. A.1). As shown in Fig. A.1, the pans are placed equidistant from the heating source (the chamber walls made of a high thermal conductivity metal like silver) and placed ∼1 cm apart from each other such that the heat flow in one pan does not affect the other. Small sample sizes (∼1–20 mg) are required to fit in the pans, and small samples also minimize the thermal resistances between the sample and the pan, which prevents thermal gradients from developing within the sample. To maintain thermal equilibrium between the walls of the DSC cell (heating source) and the sample and reference pans, non-reactive dry gases like nitrogen and argon are passed through the DSC cell. Excellent thermal contact between the pan and the sensor pedestal connected to the area thermocouple is required. This is done by ensuring that the area (∼7 mm diameter) of the base of the pans is about the same as the sensor pedestal area, and the pans are centered on the sensors. The pan and sensor pedestal surfaces should be flat and free of contamination. Al-Qatami et al. observed that pan-sensor placement can affect the heat capacity measurements done on biomaterials.[35] We also directly observed that using an autosampler instead of manually placing the pans reduced the heat flow discrepancy on running the same empty pan (Fig. S1 supplementary information). Figure A.1 shows a simplified version of the circuit model by Danley alongside a physical schematic. This model corresponds to the sample + pan + calorimeter system on the reference and sample sides. The total heat flowing into the sensor is a combination of the heat flow from the cell wall, heat capacity of the pans and sensors, and heat generated by the sample. The measured temperatures and the calculated heat flow is dependent on the thermal resistances (denoted by red bars in Fig. A.1) in the path of heat flow. Major thermal resistances include the resistance between sample and pan ($R_{P\text{-}s}$), pan and sensor ($R_{P\text{-}sensor}$) and the sensor resistance (R_{Sensor}), which also include the DSC cell's other internal resistances. Among these, the $R_{P\text{-}S}$ and $R_{P\text{-}Sensor}$ can be minimized by (1) selecting high thermal conductivity materials for pan construction with low wall thickness, and (2) keeping the pan base flat through the test, i.e. matching the coefficient of thermal expansion of the pan with the sensor material, ensuring that the sample has adequate contact with the pan base and is free of contamination. The DSC cell's material thermal resistances are treated as negligible here because of the high thermal conductivities of the materials used construction. In this representation the effect of the heat capacities of the sensors are not considered, as they can be independently measured via sapphire standards. Most DSCs have the sensor heat capacities predetermined and they are used directly as an adjustment factor in the empty cell (no pans) calibration step.

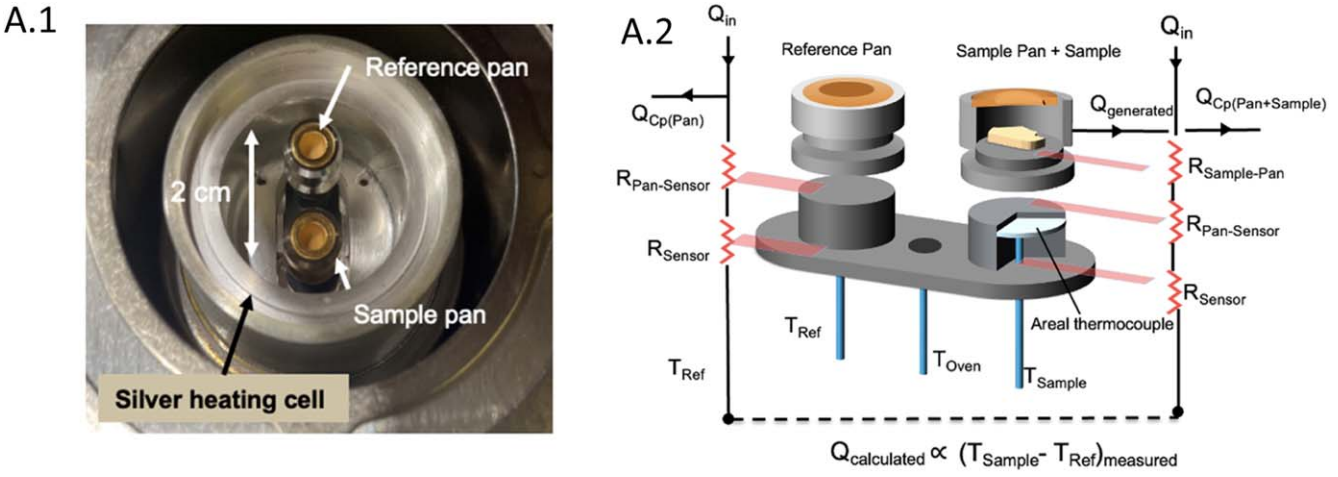

Figure A1. (A.1) A heat flux DSC cell showing reference and sample pans placed on the sensor pedestals, equidistant from the center of the cell and from the inner walls of the silver cell encasing the heating element, (A.2) schematic showing the heat flow paths and resistances involved in the temperature measurement.

ORCID

Bhuvsmita Bhargava https://orcid.org/0009-0007-1268-6635
Nathan Brenner Johnson https://orcid.org/0000-0002-1360-110X
Loraine Torres-Castro https://orcid.org/0000-0002-9267-8489
Paul Albertus https://orcid.org/0000-0003-0072-0529

References

1. T. Inoue and K. Mukai, "Are all-solid-state lithium-ion batteries really safe?–Verification by differential scanning calorimetry with an all-inclusive microcell." *ACS Appl. Mater. Interfaces*, **9**, 1507 (2017).
2. A. M. Bates, Y. Preger, L. Torres-Castro, K. L. Harrison, S. J. Harris, and J. Hewson, "Are solid-state batteries safer than lithium-ion batteries?" *Joule*, **6**, 742 (2022).
3. N. B. Johnson, B. Bhargava, J. Chang, S. Zaman, W. Schubert, and P. Albertus, "Assessing the thermal safety of a Li metal solid-state battery material set using differential scanning calorimetry." *ACS Appl. Mater. Interfaces*, acsami.3c13344 (2023).
4. Y. Wu, J. Xu, P. Lu, J. Lu, L. Gan, S. Wang, R. Xiao, H. Li, L. Chen, and F. Wu, "Thermal stability of sulfide solid electrolyte with lithium metal." *Adv. Energy Mater.*, **13**, 2301336 (2023).
5. B. S. Vishnugopi, M. T. Hasan, H. Zhou, and P. P. Mukherjee, "Interphases and electrode crosstalk dictate the thermal stability of solid-state batteries." *ACS Energy Lett.*, **8**, 398 (2023).
6. X. Rui et al., "Distinct thermal runaway mechanisms of sulfide-based all-solid-state batteries." *Energy Environ. Sci.*, **16**, 3552 (2023).
7. H. Chung and B. Kang, "Mechanical and thermal failure induced by contact between a $Li_{1.5}Al_{0.5}Ge_{1.5}(PO_4)_3$ solid electrolyte and Li metal in an all solid-state Li cell." *Chem. Mater.*, **29**, 8611 (2017).
8. N. Johnson and P. Albertus, "Modeling thermal behavior and safety of large format all-solid-state lithium metal batteries under thermal ramp and short circuit conditions." *J. Electrochem. Soc.*, **169**, 060546 (2022).
9. S. Wang, Y. Wu, T. Ma, L. Chen, H. Li, and F. Wu, "Thermal stability between sulfide solid electrolytes and oxide cathode." *ACS Nano*, **16**, 16158 (2022).
10. H. Wang et al., "Fire and explosion characteristics of vent gas from lithium-ion batteries after thermal runaway: a comparative study." *eTransportation*, **13**, 100190 (2022).
11. D. D. MacNeil and J. R. Dahn, "Test of reaction kinetics using both differential scanning and accelerating rate calorimetries as applied to the reaction of Li_xCoO_2 in non-aqueous electrolyte." *J. Phys. Chem. A*, **105**, 4430 (2001).
12. R. C. Shurtz and J. C. Hewson, "Review—Materials science predictions of thermal runaway in layered metal-oxide cathodes: a review of thermodynamics." *J. Electrochem. Soc.*, **167**, 090543 (2020).
13. Y. Baba, "Thermal stability of Li_xCoO_2 cathode for lithium ion battery." *Solid State Ionics*, **148**, 311 (2002).
14. Z. Chen, Y. Qin, Y. Ren, W. Lu, C. Orendorff, E. P. Roth, and K. Amine, "Multi-scale study of thermal stability of lithiated graphite." *Energy Environ. Sci.*, **4**, 4023 (2011).
15. Z. Zhang, D. Fouchard, and J. R. Rea, "Differential scanning calorimetry material studies: implications for the safety of Lithium-Ion cells." *J. Power Sources*, **70**, 16 (1998).
16. H. M. Barkholtz, Y. Preger, S. Ivanov, J. Langendorf, L. Torres-Castro, J. Lamb, B. Chalamala, and S. R. Ferreira, "Multi-scale thermal stability study of commercial lithium-ion batteries as a function of cathode chemistry and state-of-charge." *J. Power Sources*, **435**, 226777 (2019).
17. D. Puthusseri, M. Parmananda, P. P. Mukherjee, and V. G. Pol, "Probing the thermal safety of li metal batteries." *J. Electrochem. Soc.*, **167**, 120513 (2020).
18. C. Lenz, J. Hennig, W. Tegethoff, H-G. Schweiger, and J. Koehler, "Analysis of the interaction and variability of thermal decomposition reactions of a Li-Ion battery cell." *J. Electrochem. Soc.*, **170**, 060523 (2023).
19. A. Bates, L. Torres-Castro, P. Albertus, P. P. Mukherjee, J. Jeevarajan, N. Johnson, Tang, and , "A multi-scale framework for advancing battery safety through early calorimetric analysis of materials and components." *The Electrochemical Society Interface*, **33**, 69 (2024).
20. W-S. Yoon, K. Y. Chung, M. Balasubramanian, J. Hanson, J. McBreen, and X-Q. Yang, "Time-resolved XRD study on the thermal decomposition of nickel-based layered cathode materials for Li-Ion batteries." *J. Power Sources*, **163**, 219 (2006).
21. A. Kriston, I. Adanouj, V. Ruiz, and A. Pfrang, "Quantification and simulation of thermal decomposition reactions of Li-Ion battery materials by simultaneous thermal analysis coupled with gas analysis." *J. Power Sources*, **435**, 226774 (2019).
22. J. A. Jeevarajan, B. Duffield, and J. C. Orieukwu, "Safety of Lithium-Ion cells at different states of charge." *In Space Safety is No Accident*, ed. T. Sgobba and I. Rongier (Springer International Publishing)131 (2015).
23. S. Sharifi-Asl, J. Lu, K. Amine, and R. Shahbazian-Yassar, "Oxygen release degradation in Li-Ion battery cathode materials: mechanisms and mitigating approaches." *Adv. Energy Mater.*, **9**, 1900551 (2019).
24. L. Wang, T. Maxisch, and G. Ceder, "A first-principles approach to studying the thermal stability of oxide cathode materials." *Chem. Mater.*, **19**, 543 (2007).
25. R. C. Shurtz, "A thermodynamic reassessment of lithium-ion battery cathode calorimetry." *J. Electrochem. Soc.*, **167**, 140544 (2020).
26. S. Vyazovkin, K. Chrissafis, M. L. Di Lorenzo, N. Koga, M. Pijolat, B. Roduit, N. Sbirrazzuoli, and J. J. Suñol, "ICTAC kinetics committee recommendations for collecting experimental thermal analysis data for kinetic computations." *Thermochim. Acta*, **590**, 1 (2014).
27. R. L. Danley, "New heat flux DSC measurement technique." *Thermochim. Acta*, **395**, 201 (2002).
28. M. Schubnell, "Temperature and heat flow calibration of A DSC-instrument in the temperature range between −100 and 160 °C." *J. Therm. Anal. Calorim.*, **61**, 91 (2000).
29. E37 Committee, *Practice for Heat Flow Calibration of Differential Scanning Calorimeters* (ASTM International).
30. S-M. Bak, E. Hu, Y. Zhou, X. Yu, S. D. Senanayake, S-J. Cho, K-B. Kim, K. Y. Chung, X-Q. Yang, and K-W. Nam, "Structural changes and thermal stability of charged $LiNi_x$ $Mn_yCo_zO_2$ cathode materials studied by combined In Situ time-resolved XRD and mass spectroscopy." *ACS Appl. Mater. Interfaces*, **6**, 22594 (2014).
31. R. C. Shurtz, Y. Preger, L. Torres-Castro, J. Lamb, J. C. Hewson, and S. Ferreira, "Perspective—From calorimetry measurements to furthering mechanistic understanding and control of thermal abuse in Lithium-Ion cells." *J. Electrochem. Soc.*, **166**, A2498 (2019).
32. S. I. Stoliarov and R. N. Walters, "Determination of the heats of gasification of polymers using differential scanning calorimetry." *Polym. Degrad. Stab.*, **93**, 422 (2008).
33. W. J. Frederick and C. C. Mentzer, "Determination of heats of volatilization for polymers by differential scanning calorimetry." *J of Applied Polymer Sci*, **19**, 1799 (1975).
34. G. Agarwal and B. Lattimer, "Method for measuring the standard heat of decomposition of materials." *Thermochim. Acta*, **545**, 34 (2012).
35. O. Al-Qatami and G. Mazzanti, "The effect of the sample pan position on the determination of the specific heat capacity for lipid materials using heat flux DSC." *Thermochim. Acta*, **710**, 179148 (2022).